Driving the TING model with GAIM electron densities: Ionospheric effects on the thermosphere

G. Jee,[1,3] A. G. Burns,[1] W. Wang,[1] S. C. Solomon,[1] R. W. Schunk,[2] L. Scherliess,[2] D. C. Thompson,[2] J. J. Sojka,[2] and L. Zhu[2]

Received 31 May 2007; revised 12 November 2007; accepted 12 December 2007; published 18 March 2008.

[1] In order to study the effects of ionospheric plasma densities on the thermosphere, the electron and O^+ densities in the Thermosphere Ionosphere Nested Grid (TING) model were replaced by electron densities from the Global Assimilation of Ionospheric Measurements (GAIM) model at pressure level z = 0 (about 210 $\sim$ 230 km altitude) and above. This GAIM-derived TING model (G-TING) was then run for the period 1–4 April 2004. The TING model was also run as a stand-alone coupled model (S-TING), without using the GAIM electron densities, for the same period. The resulting thermospheric responses from the two simulations were compared at around the *F* region peak altitude. There was an extended quiet period during this interval followed by a moderate geomagnetic storm ($K_p \sim 6.0$). The ingestion of the GAIM electron densities had little effect on the neutral temperature and composition during the quiet period before the storm, but there were noticeable global effects on the neutral winds, mainly as a result of changes in the ion drag force. During disturbed periods, changed electron densities produced much more significant effects on the global thermosphere. The increased auroral electron densities enhanced the Joule heating rate, in addition to the ion drag, which resulted in significant global changes not only in the neutral winds, but also in the neutral temperature and composition. The results of our study confirm that having correct ionospheric plasma densities is critical to accurately predicting the thermosphere in the coupled thermosphere-ionosphere model.

Citation: Jee, G., A. G. Burns, W. Wang, S. C. Solomon, R. W. Schunk, L. Scherliess, D. C. Thompson, J. J. Sojka, and L. Zhu (2008), Driving the TING model with GAIM electron densities: Ionospheric effects on the thermosphere, *J. Geophys. Res.*, *113*, A03305, doi:10.1029/2007JA012580.

1. Introduction

[2] The ionosphere and thermosphere are so tightly coupled chemically, dynamically, and electrodynamically that it is almost impossible to treat them as two separate systems. The plasma density distribution of the ionosphere is greatly affected by neutral parameters such as neutral composition (e.g., O/N_2), neutral temperature and neutral winds. During a geomagnetic storm, neutral composition and global thermospheric circulation are significantly disturbed due to atmospheric heating, which results in the expansion of the neutral atmosphere and, hence, stronger pressure gradients and winds at high latitudes. These changes in neutral composition and winds can have a considerable effect on plasma densities, producing large stormtime variations in the global ionosphere [*Buonsanto*, 1999 and references therein]. Even during geomagnectically quiet times, these thermospheric parameters play an important role in, for instance, the maintenance of the nighttime ionosphere by neutral winds [*Titheridge*, 1968, 1995] and producing ionospheric variations such as the winter anomaly and semiannual anomaly [*Rishbeth*, 1998; *Rishbeth et al.*, 2000]. In addition to the chemical and dynamical effects, the electrical properties of the ionosphere can be greatly influenced by the thermosphere: the neutral winds can induce ionospheric dynamo electric fields by moving ions and electrons across the geomagnetic field lines in different directions [*Rishbeth*, 1997]. The resulting dynamo electric fields are responsible for many important ionospheric phenomena such as the equatorial anomaly and equatorial electrojet.

[3] On the other hand, the thermosphere is also significantly influenced by the existence of the ionosphere, despite the fact that the ionospheric plasma is only a minor constituent in the upper atmosphere (about 0.1% or less of the thermospheric neutral density at the F_2 peak). What follows is the brief review of the ionospheric influences on the thermosphere, which can readily be skipped by the experienced readers.

[1]High Altitude Observatory, National Center for Atmospheric Research, Boulder, Colorado, USA.
[2]Center for Atmospheric and Space Sciences, Utah State University, Logan, Utah, USA.
[3]Now at Korea Polar Research Institute, Incheon, Korea.

0148-0227/08/2007JA012580

1.1. How the Ionosphere Influences the Thermosphere: A Brief Review

[4] The ionospheric influences on the thermosphere often appear in the form of ion drag in the momentum equations and Joule heating in the neutral energy equation [*Zhu et al.*, 2005]. When neutral particles move with a mean velocity of $\mathbf{v}_n$ through the ionospheric plasma with the mean velocity of $\mathbf{v}_i$, the neutrals experience an ion drag force $\mathbf{F}_d$ [*Kelley*, 1989]:

$$\mathbf{F}_d = -\rho_n \nu_{ni}(\mathbf{v}_n - \mathbf{v}_i) \quad (1)$$

where $\rho_n = m_n n_n$ is the mass density of neutrals and ν_{ni} is the neutral-ion momentum transfer collision frequency (electrons are ignored due to their small mass, compared with neutral and ion masses). The ions are largely constrained to move parallel to the geomagnetic field when the neutral-ion collision frequency is much smaller than the ion gyrofrequency, which generally occurs above *E*-region altitudes. In this altitude region, therefore, instead of freely moving with neutrals under the frictional force, the ions can exert a steady drag on the motion of the neutrals perpendicular to the magnetic field.

[5] Ion drag can have a considerable influence on the thermosphere. In the equatorial region, there is a net eastward motion of the thermosphere, which is called superrotation, and it can be explained by the day/night changes of the ion drag, further enhanced by the polarization electric fields generated by the *F*-region dynamo [*King-Hele*, 1964; *Rishbeth*, 1979, 2002; *Kelley*, 1989]. This effect of ion drag is related to the neutral motion perpendicular to the geomagnetic field. However, ion drag can also affect neutral motion parallel to the field line in the equatorial region [*Maruyama et al.*, 2003]. One of the results of their model simulation study was that, in the vicinity of the equatorial anomaly region, the poleward field-aligned ion motion and the resultant ion drag accelerates the neutral wind and drives a divergence at the geomagnetic equator, which also results in a temperature decrease as a result of adiabatic cooling.

[6] In the auroral regions, ion drag can act as a driver for the neutral winds when there is strong ion convection, which leads to a continuous acceleration of the neutrals in the direction of the ion drift. The resulting neutral circulation pattern, to a certain extent, resembles the ion convection pattern [*Killeen and Roble*, 1984; *Zhang and Shepherd*, 2000]. Furthermore, the ionosphere-driven neutral convection can also influence the ionosphere by the so-called "flywheel" effect when the magnetospheric electric field driving ion convection is suddenly weakened [*Lyons et al.*, 1985; *Deng et al.*, 1991, 1993].

[7] In addition to momentum transfer from convecting ions to neutrals, energy transfer also occurs between them. The collisions between convecting plasma and neutrals in the auroral region lead to the acceleration of the neutral particles not only in the direction of the drifting plasma (bulk flow acceleration), but also by heating the neutral atmosphere. Alternatively, this can be thought of as the energy of the magnetospheric electric field **E** being transferred to the ionospheric plasma and dissipated into the thermosphere via collisions with neutrals at a rate

$$Q = \mathbf{J} \cdot \mathbf{E} = \sigma_P E'^2 \quad (2)$$

where Q is the heating rate per unit volume, σ_P is the Pedersen conductivity, and $\mathbf{E}' = \mathbf{E} + \mathbf{u}_n \times \mathbf{B}$ denotes the externally applied electric field from the magnetosphere (**E**) and the neutral wind dynamo ($\mathbf{u}_n \times \mathbf{B}$). The dynamo electric field works to reduce the magnetospheric convection electric field and it can influence how much of magnetospheric energy is deposited into the ionosphere-thermosphere system [*Prölss*, 2004; *Thayer*, 2000; *Cierpka et al.*, 2000]. One of the main consequences of Joule heating, in particular during disturbed times, is the neutral temperature increase, which causes substantial impacts on the global neutral circulation and thereby thermospheric dynamics and composition.

1.2. Models

[8] Having described the impact of ion drag and Joule heating on the ionosphere-thermosphere (IT) coupling, it is necessary to describe how this coupling relates to ion density. The ion-neutral momentum transfer collision frequency (ν_{ni}) in equation (1) and the Pedersen conductivity (σ_P) in equation (2) are roughly proportional to the ion density. That is, for a given ion-neutral relative velocity and external electric field, the ion drag and Joule heating, and thus their impact on the thermosphere are crucially dependent on the ionospheric plasma density [*Killeen*, 1987; *Schunk and Nagy*, 2000]. In this paper, we study the sensitivity of the thermosphere to ionospheric plasma density variations, especially in the *F*-region, as a result of the IT coupling processes. For this purpose, we performed a simulation study of thermospheric responses to changes in the ionospheric plasma density in a coupled IT model for various geophysical conditions on a global scale. The plasma density changes in the coupled model are achieved by replacing the electron and ion densities of the model with the electron densities from an ionospheric data assimilation model. In this section, we will briefly describe the models used for this study, the Thermosphere Ionosphere Nested Grid (TING) model as a coupled IT model and the USU Global Assimilation of Ionospheric Measurements (GAIM) model as an ionospheric data assimilation model.

1.2.1. TING Model

[9] The TING model is an extension of the NCAR Thermosphere-Ionosphere General Circulation Model (TIGCM) [*Roble et al.*, 1988; *Wang et al.*, 1999]. Within the TIGCM coarse grid ($5^\circ \times 5^\circ$), one or more levels of nested grids can be inserted in regions of interest to simulate mesoscale and micro-scale processes occurring in the thermosphere-ionosphere system. The TING model is a time-dependent, three-dimensional model that solves the momentum, energy and continuity equations of major and minor neutral species of the upper atmosphere, self-consistently with the O^+ transport equations. Chemical equilibrium is assumed to obtain densities of other ions and electrons. The TING model has 25 constant pressure levels in the vertical between approximately 97 and 500 km altitude with a vertical resolution of 2 grid points per scale height. The upper and lower boundary conditions of the TING model are specified basically by assuming diffusive and chemical equilibriums, respectively. The model outputs for the neutral thermosphere are global distributions of neutral gas temperature, winds, mass mixing ratios of the major constituents, N_2, O_2, and O, and the mass mixing

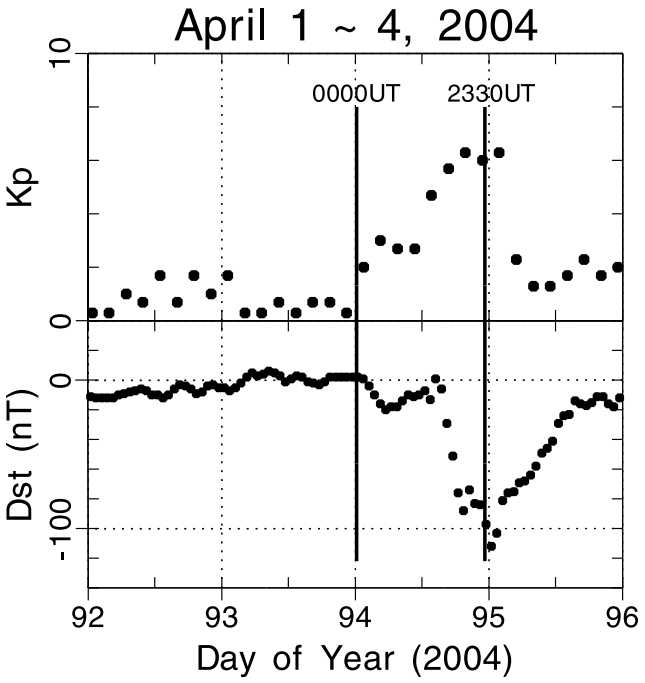

Figure 1. April 2004 period in K_p (top) and D_{st} (bottom) with two universal times (UT) for this study, which are indicated by vertical lines for quiet (0000 UT of day 94) and disturbed (2330 UT of day 94) time periods.

ratios of the minor neutral gas constituents, $N(^2D)$, $N(^4S)$, *NO*, *He*, and *Ar*. For the ionosphere, global distributions of electron and ion temperatures, O^+, O_2^+, NO^+, N_2^+, N^+, and electron densities are calculated.

1.2.2. GAIM Model

[10] The GAIM model is a data assimilation model for the ionosphere that has been developed to provide a specification of the ionospheric plasma distribution by combining a physics-based model and a variety of observations from the ground and space, via a Kalman filter technique [*Schunk et al.*, 2004; *Scherliess et al.*, 2006]. The Gauss-Markov Kalman Filter (GMKF) model (one of the two versions of the GAIM model and thereafter simply called the GAIM model) uses the physics-based ionosphere forecast model (IFM) to provide background ionospheric densities and a statistical Gauss-Markov process to propagate ion density perturbations and the associated errors with time. GAIM can assimilate a variety of measurement types from variable numbers of satellites and ground stations. Only three data types are assimilated for this study: line-of-sight Total Electron Content (TEC) measurements between 162 ground stations and GPS satellites, bottomside electron density profiles from 14 ionosondes, and in situ electron densities from 3 DMSP satellites. These data are assimilated by the model from +60° to −60° geographic latitude. Assimilated data affect the GAIM result outside the assimilation region owing to correlation distances in the model. Hence above about ±70°, the GAIM output is purely from the background ionospheric model (IFM). Output from the GAIM model is a global 3-D time-varying distribution of electron density from 90 to 1400 km [*Scherliess et al.*, 2006; *Thompson et al.*, 2006]. This output has been interpolated onto the TING pressure coordinates for this study.

[11] In the next section, the procedure for this simulation study will be described, which is followed by the description of the differences in electron densities from the two models in section 3. The results of our study will be presented by describing how the differences in electron densities affect thermospheric structures in section 4. Finally, these results will be discussed and summarized in sections 5 and 6, respectively.

2. Procedure

[12] The electron and O^+ densities in the TING model were continually replaced at every time step by electron densities from the GAIM model. This procedure was performed only at the pressure level z = 0 and above (e.g., height greater than approximately 210 ~ 230 km), where O^+ is the dominant ion species, since the GAIM model produces only electron densities and replacing O^+ with the electron densities below this pressure level is not consistent with the chemistry in the TING model. By restricting the replacement in this manner, the changes of ionospheric plasma density were applied only in the *F*-region and above in the TING model and, therefore, this study will be focused on this altitude region.

[13] The period for this study is the early April 2004 period, which includes a moderate geomagnetic storm ($K_p \approx 6.0$) that follows an extended quiet time period for low solar activity (F10.7 ≈ 105). Figure 1 shows the K_p (top) and D_{st} (bottom) indices for this period. The two UTs for this study are indicated by vertical lines for quiet (0000 UT of day 94) and disturbed (2330 UT of day 94) conditions. The electron and O^+ densities in the TING model were continually replaced with the GAIM electron densities at a 15-min time interval during the course of model runs from 1 to 4 April for pressure level of z = 0 and above. Although the TING model has a 3-min time step in this study, the electron and O^+ densities were replaced by using the same electron densities for 15 min, since the GAIM outputs have a 15-min time interval. From the TING model runs derived with these GAIM electron densities (G-TING), various neutral parameters were computed and then compared with the same neutral parameters computed from the stand-alone TING model run (S-TING).

[14] Our study is focused on the altitude regions around the F_2 peak. Since the rates of many ionospheric processes (photoionization, chemical loss and diffusion of the ionospheric plasma) depend critically on the neutral density (or pressure), it can be assumed that the F_2 peak tends to be nearly at a constant pressure level for a given local time and location, regardless of season, solar cycle, and geomagnetic activity [*Garriott and Rishbeth*, 1963; *Rishbeth and Edwards*, 1989]. It is concluded from their studies that thermal expansion and contraction caused by the temperature changes in the neutral atmosphere do not affect the pressure level of the F_2 peak. However, other physical processes such as the neutral winds and electric field can cause changes in the pressure level at which the F_2 peak occurs. There are actually fluctuations of ±1 ~ 2 pressure levels in the F_2 peak altitude with local time, latitude, and geomagnetic activity changes in our study period. Despite this issue, the results of this study will be presented on the

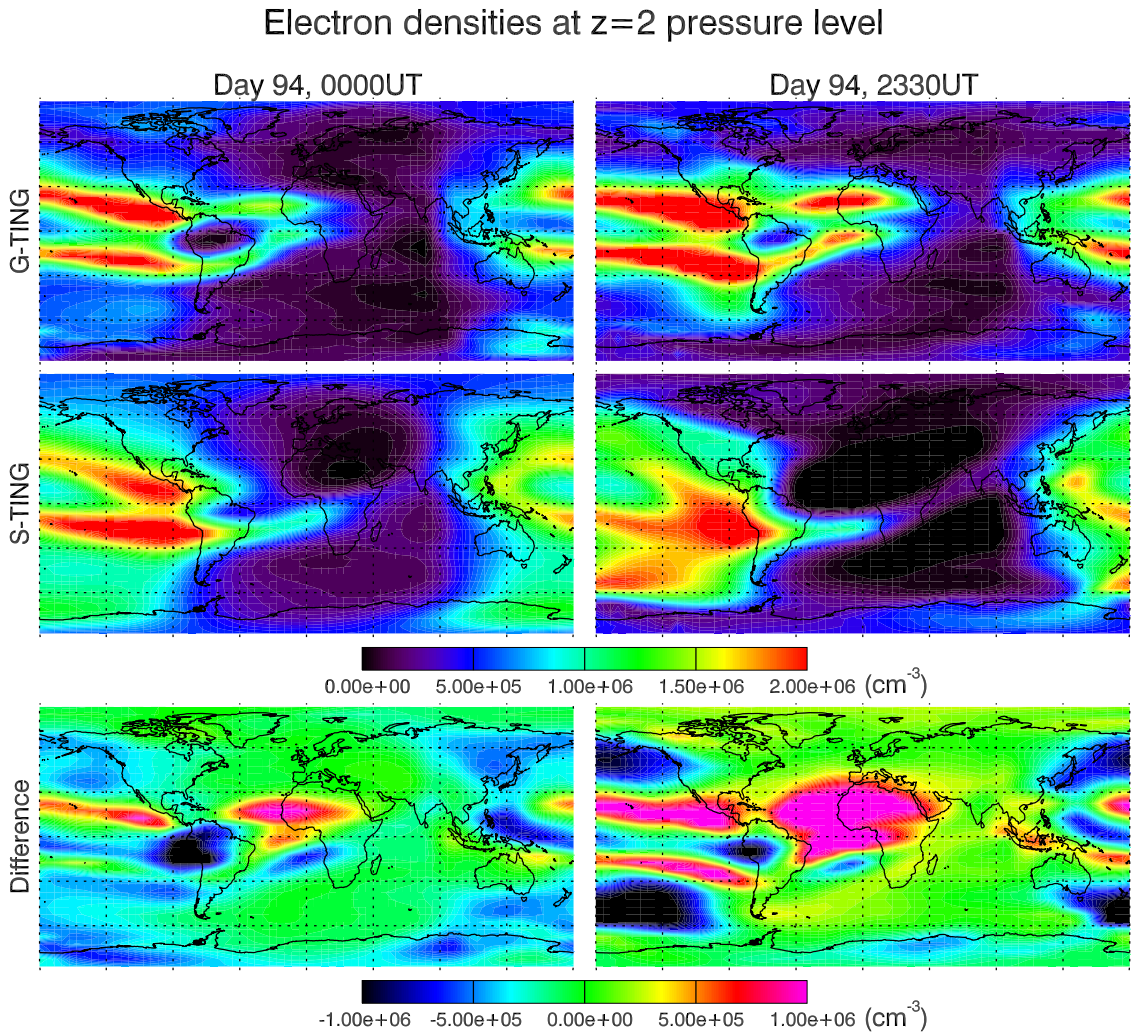

Figure 2. The global maps of the electron densities at z = 2 pressure level for the quiet (left) and disturbed (right) times. The electron densities from the GAIM-driven and stand-alone TING models are displayed in the top and middle panels, respectively, and the bottom panels display the difference between them (G-TING-S-TING).

z = 2 pressure level (about 300 $\sim$ 320 km altitude) as a representative pressure level for the F_2 peak.

[15] Prior to presenting the results of this study, the differences between the F-region electron densities from the GAIM and TING models will be described in the next section to identify how much the electron densities have been changed in the TING model.

3. Differences Between GAIM and TING Electron Densities

[16] Figure 2 shows the global maps of the electron density at the z = 2 pressure level for quiet (left) and disturbed (right) times. The electron densities from the G-TING and S-TING models are displayed in the top and middle panels, respectively, and the bottom panels display the difference between them (G-TING - S-TING). During quiet times, the most evident differences appear in the equatorial region of the evening sector, where the S-TING model shows only a single density peak. At middle latitudes, the S-TING model also shows much larger electron densities during the daytime. Auroral electron densities from two models are similar in the northern hemisphere, but in the southern hemisphere the S-TING model produces mostly larger electron densities than the G-TING model.

[17] The differences during disturbed times are larger and more distinctive. The equatorial anomaly in the S-TING model is weak compared with the anomaly feature in the G-TING model, which is shown as very large positive differences in Figure 2. However, it should be remembered that the electron densities in this figure do not represent the F_2 peak densities. N_mF_2 in the stand-alone TING model gives a better description of the equatorial anomaly although it is still weaker than in the GAIM model (not shown). The daytime midlatitude region, as in the quiet time case, shows quite noticeable negative differences (G-TING < S-TING) in both hemispheres but they are particularly large in the southern hemisphere. At high latitudes, the G-TING model has larger electron densities in the northern hemisphere but slightly smaller densities in the southern hemisphere.

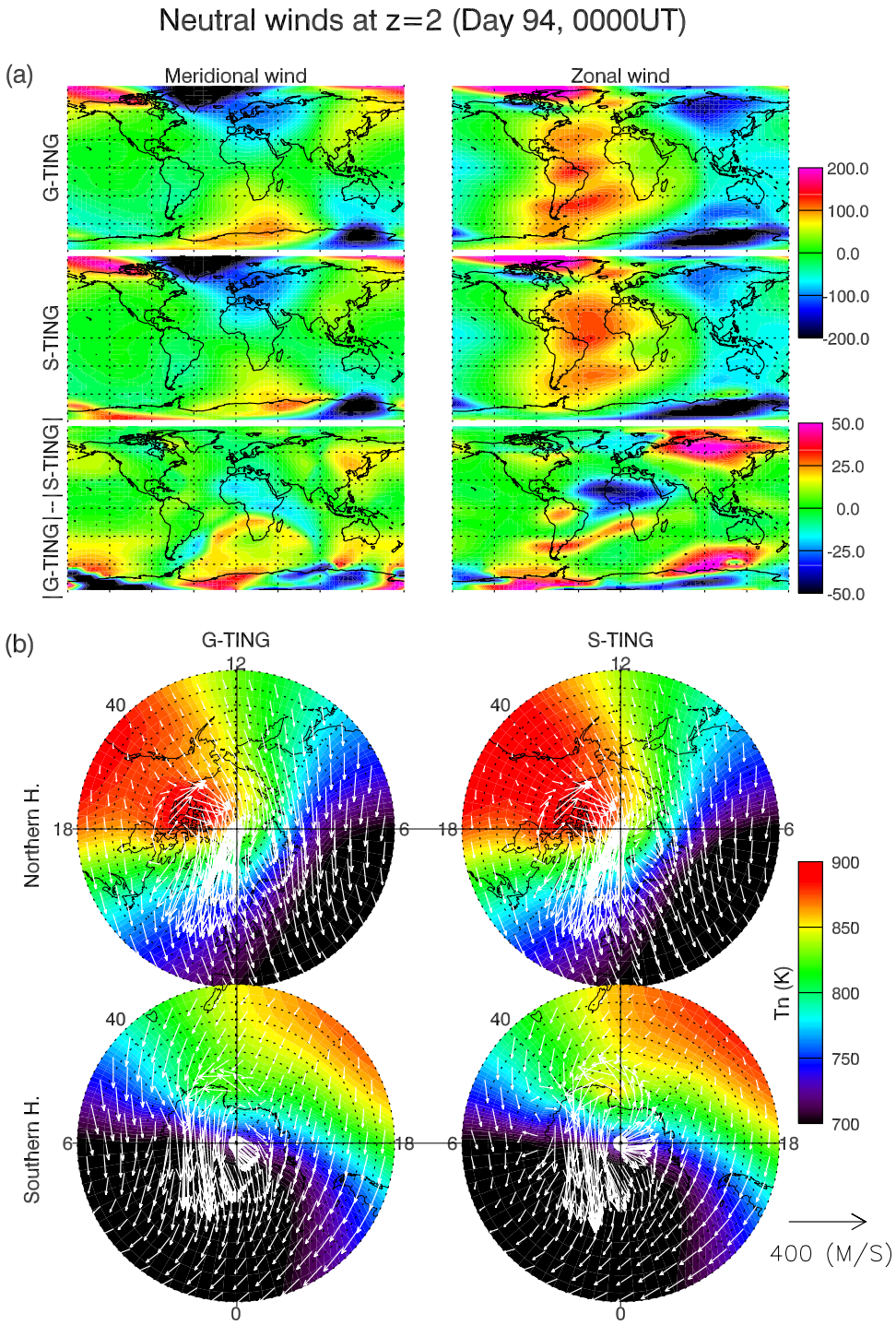

Figure 3. (a) The meridional (left) and zonal (right) winds during quiet times from the GAIM-driven TING model (top), stand-alone TING model (middle), and their differences in magnitude (bottom). (b) The same neutral winds as vectors only in the polar region (from the poles to ±40° GLAT) together with the neutral temperature, also from the G-TING (left diagrams) and S-TING (right diagrams) in the northern (top) and southern (bottom) hemispheres, separately.

[18] It should be noted that the electron density differences at high latitudes (greater than ±70°) are from the comparison between the TING model and the background ionospheric model (IFM) for GAIM, without taking account of the effects of assimilating any measurements. These differences actually reflect the model differences at high latitudes between the TING model and the ionosphere forecast model (IFM). The IFM utilizes empirical models such as the MSISE-90 model for the neutral densities and temperature [*Hedin et al.*, 1991], the HWM for the neutral winds [*Hedin et al.*, 1991], and the Heppner-Maynard model for the high-latitude electric field [*Heppner and*

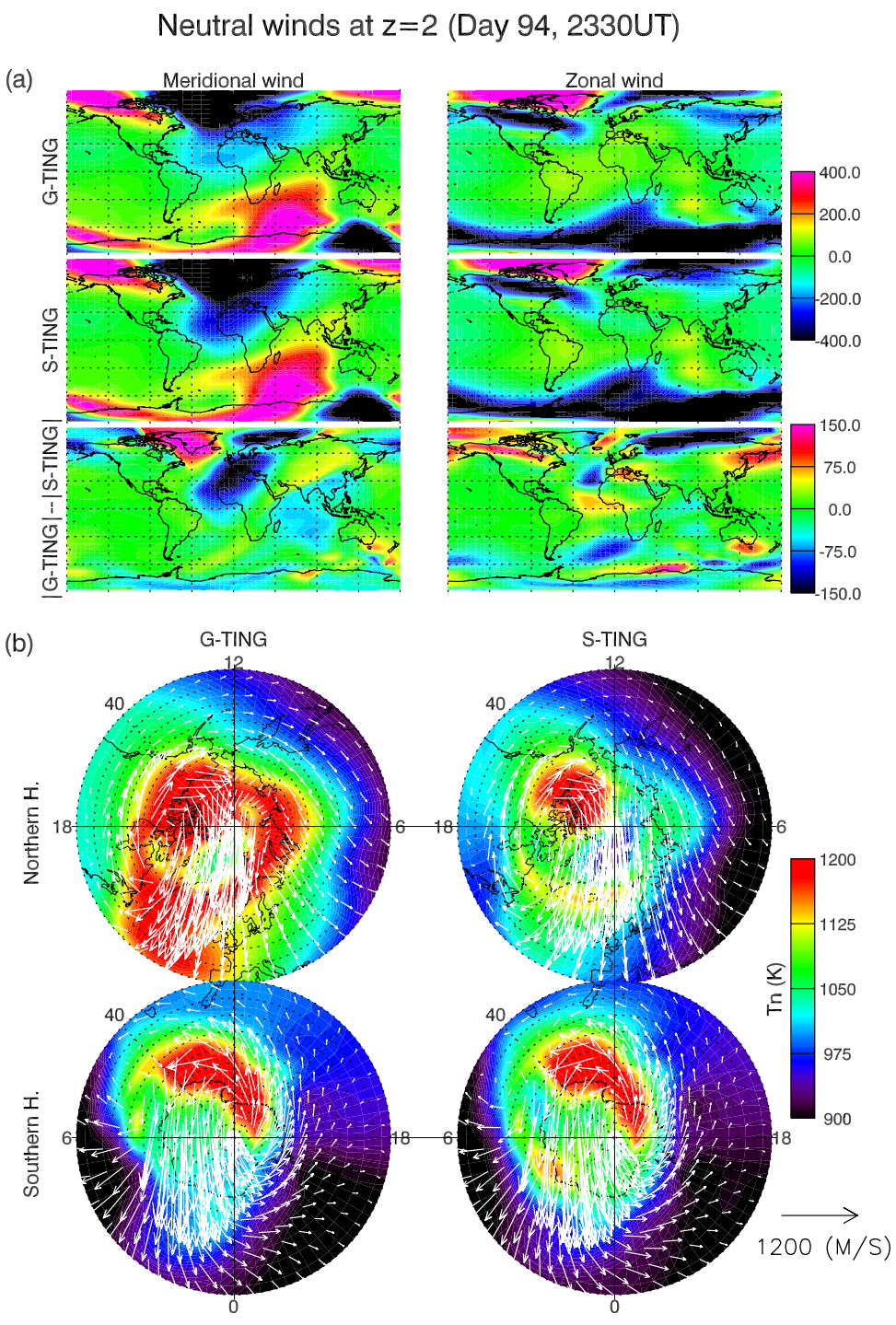

Figure 4. Same as Figure 3, but during disturbed times.

Maynard, 1987], whereas the TING model self-consistently calculates the neutral parameters by solving physical equations and utilizes the Heelis convection model for the high-latitude electric field [*Heelis et al.*, 1982]. Both TING and GAIM use the Hardy auroral precipitation model [*Hardy et al.*, 1989]. In addition to the auroral thermosphere and electric field, the differences in the auroral electron densities might be, in part, related with a resolution issue in the TING model [*Wang et al.*, 1999]. The current study uses only the low-resolution grid of the TING model (5° × 5° in latitude and longitude), which is not sufficient to accurately simulate fine structures, such as the tongue of ionization (TOI) and boundary blobs at high latitudes.

4. Results: Thermospheric Differences

[19] The electron density differences described in the previous section caused changes of the thermosphere in the TING model. However, it should be noted that the electron density differences deriving the model are not

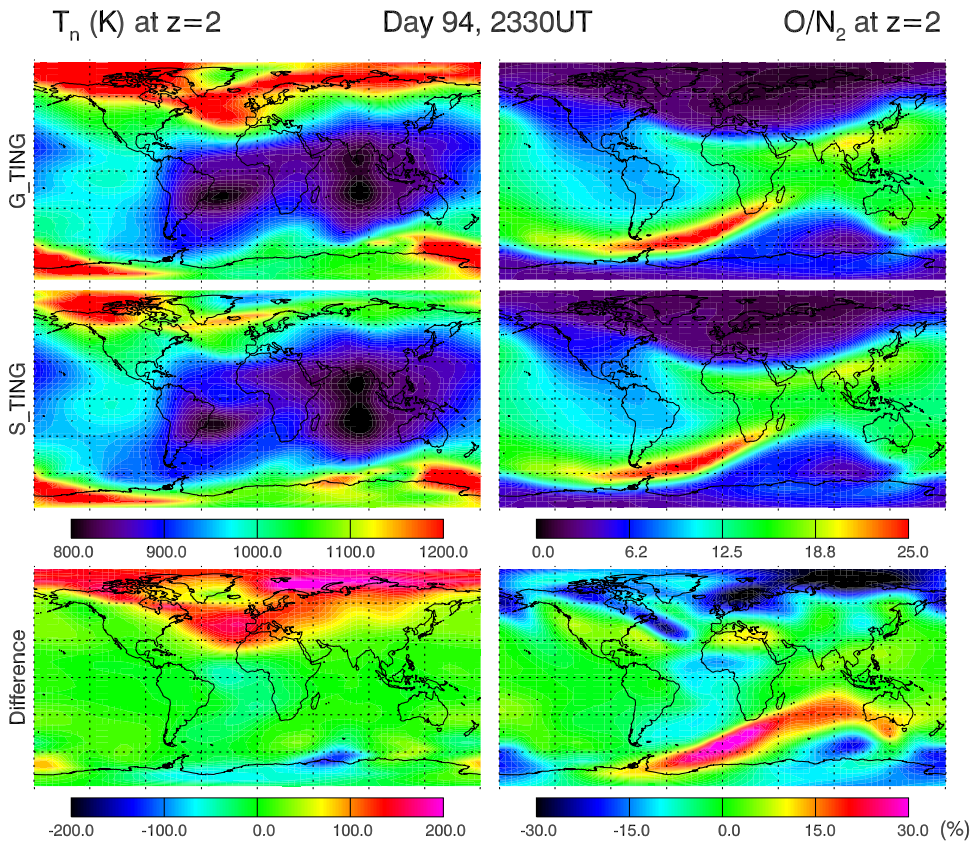

Figure 5. The neutral temperature (left) and composition (O/N_2) (right) during disturbed times from the GAIM-driven TING model (top) and the stand-alone TING model (middle). The differences [G-TING−S-TING] between the two models are presented in the bottom panels.

uniform in terms of spatial and temporal changes and the resulting effects in the thermosphere may be influenced by this nonuniformity, which is not intended to be identified in this study but rather oriented toward the global picture of the effects, particularly near the F_2 peak.

[20] During quiet times, the changes of the plasma densities in the TING model caused noticeable changes in the neutral winds, although there was little effect on thermospheric temperatures and composition. Figure 3a shows snapshots of the neutral winds from the G-TING and S-TING during quiet time (day 94, 00UT). The top panels display the meridional (left) and zonal (right) winds from the G-TING model (top), the S-TING model (middle), and their differences in magnitude (bottom panels). The differences represent the changes of the magnitude of the wind ($|\mathbf{U}_{\text{G-TING}}|-|\mathbf{U}_{\text{S-TING}}|$). The positive and negative values in the figure represent northward and southward for the meridional wind, and eastward and westward for the zonal wind. The positive values in the difference maps represent larger wind speeds from G-TING than S-TING and the negative differences represent smaller winds. There are relatively larger and more systematic changes in the zonal wind compared with those in the meridional wind. In Figure 3a, the differences in the zonal wind display distinctive decreases and increases in the equatorial eastward wind at around midnight, but significant increases of the high-latitude westward wind appear in the morning sector. For the meridional wind, the effects are very small at low latitudes, where the magnitudes of the wind itself are relatively small compared with those at higher latitudes. There are also noticeable hemispheric differences at high latitudes, particularly in the meridional wind; significantly larger differences are observed in the southern hemisphere. These rather complicated difference patterns at high latitudes can be more clearly seen in the vector plot in Figure 3b. This figure shows the same winds as Figure 3a, but in polar coordinates (greater than ±40° GLAT) plotted as a vector over the neutral temperature, also from the G-TING model (left diagrams) and the S-TING model (right diagrams) in the northern (top) and southern (bottom) hemispheres. The overall neutral wind pattern from the G-TING model is noticeably weaker than the one from the S-TING model in the southern hemisphere, but quite similar in the northern hemisphere, which corresponds to the complex difference patterns at high latitudes in Figure 3a.

[21] Much more significant changes appear in the thermosphere during disturbed times. Figure 4 shows the effects on the neutral winds in the same format as Figure 3. The wind effects during disturbed times are considerably larger than the quiet time changes, particularly, at high latitudes for both the meridional and zonal winds (Figure 4a). There are much more significant changes in the northern hemisphere than in the southern hemisphere, which appears as stronger neutral winds in the G-TING model (Figure 4b). Note that the large hemispheric differences in the auroral zonal wind shown in Figure 4a are due to the different

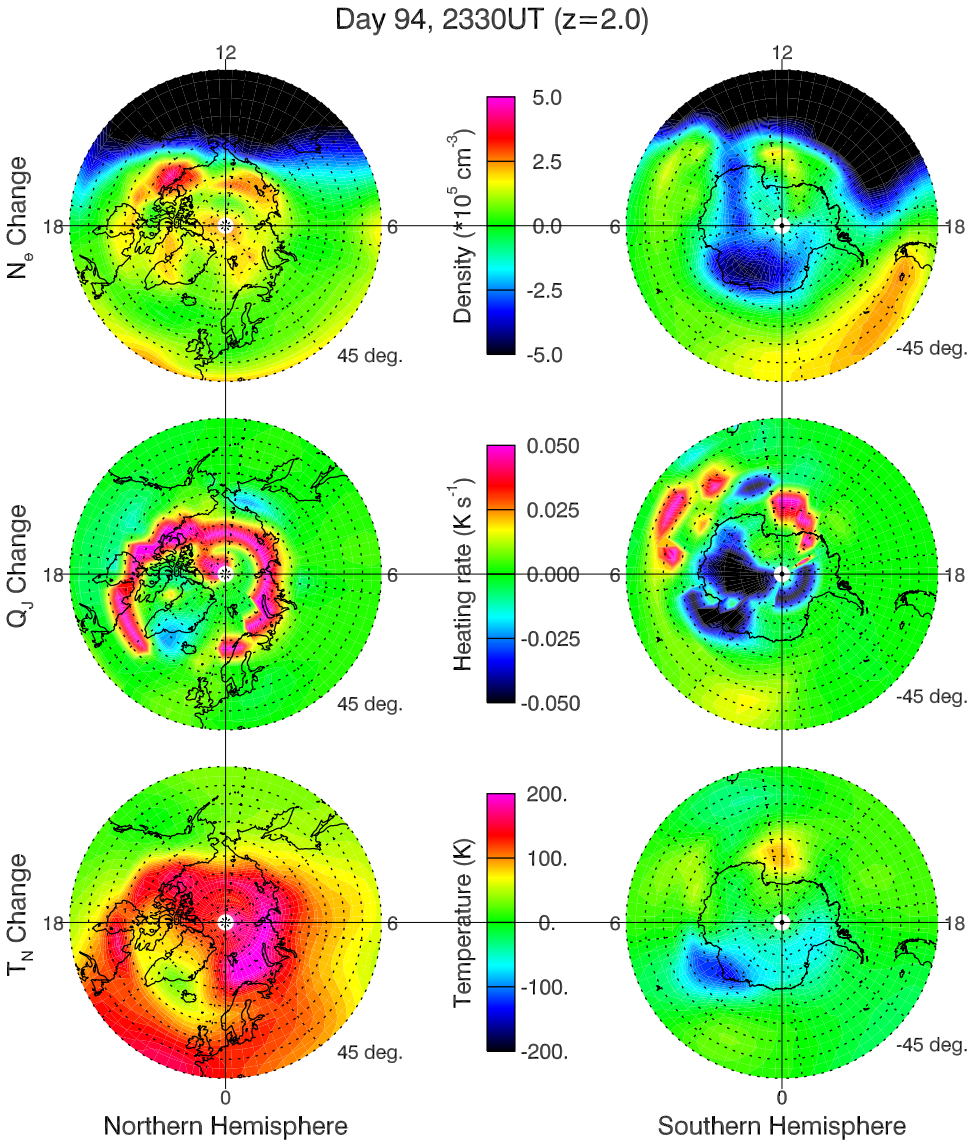

Figure 6. The electron density differences (top), corresponding Joule heating (middle) and temperature (bottom) changes are presented only at high latitudes greater than ±45° in the polar coordinates. The northern and southern hemispheres are displayed in the left and right panels, respectively. The differences are [G-TING−S-TING].

geographic locations of the geomagnetic poles in the northern and southern hemispheres, which causes relatively different geographic locations of sunward and anti-sunward winds around the auroral region in both hemispheres (see Figure 4b).

[22] Changing the ion density produced significant effects on the neutral temperature and composition (O/N_2) during disturbed times and they are displayed in Figure 5. This figure shows the temperatures (left) and O/N_2 ratio (right) from the two model runs and their differences in the bottom panels. The neutral temperatures are quite significantly enhanced, up to 200°K, in the northern hemisphere, but the changes are relatively small in the southern hemisphere. These temperature changes are most probably related to the Joule heating changes that are shown in Figure 6. In this figure, electron density differences (top) and the corresponding temperature changes (bottom) are also displayed in polar coordinates (greater than ±45°) in addition to the relevant Joule heating changes (middle). The northern and southern hemispheres are displayed in the left and right columns, respectively. The electron density differences are the same differences at high latitudes as shown in Figure 2, but only in different coordinates. It is evident in Figure 6 that the changes in electron densities, Joule heating rates, and the neutral temperature are closely correlated with each other.

[23] Finally, the O/N_2 ratio in Figure 5 also shows noticeable changes in the both hemispheres. In the difference map presented as percentage changes of O/N_2 between the G-TING model and the S-TING model, there are mostly negative changes at high latitudes, particularly strong (up to 30%) in the northern hemisphere, but the low-latitude region shows very small changes. Note that there are also

quite noticeable positive changes in the southern hemisphere, mostly during nighttime.

5. Discussion

5.1. Quiet Periods

[24] The main consequence of changing the ionospheric plasma densities during quiet geomagnetic conditions is to change ion drag effects on the thermosphere. Since the ion-neutral collision frequency is approximately proportional to the ion density [*Rishbeth*, 1979], ion density changes in the TING model affect the ion drag force on the neutrals, primarily causing the changes of the neutral winds that are seen in Figure 3. The overall effects appear to be more distinctive in the zonal wind than in the meridional wind. At low latitudes, the magnetic field is nearly horizontal and it tends to be in the meridional direction in the horizontal plane (i.e., the declination angle is relatively small at low latitudes). Therefore the zonal wind is in a nearly perpendicular direction to the magnetic field and experiences stronger ion drag than the meridional wind. It should also be noted that the ion drag effect on the meridional wind becomes even smaller due to the relatively small meridional wind compared with the corresponding zonal winds at low latitudes (Figure 3a). The nighttime differences in the zonal wind show a remarkable correlation with the corresponding electron density differences. This correlation seems to be a direct consequence of the ion drag effect; that is, increased ion density reduced the wind by increasing ion drag and vice versa. However, the daytime zonal wind at low latitudes shows little change in spite of large ion density changes because the magnitude of daytime winds is very small compared with the nighttime winds.

[25] At high latitudes, ion drag still has a strong influence on the neutral winds during quiet times, but in a way opposite from the lower-latitude effects. As shown in Figure 3b, the decreased ion densities in the southern hemisphere (Figure 2) reduced the ion drag, which weakened the resulting neutral winds. The strong and rather complex changes of the meridional and zonal winds at southern high latitudes are mainly the result of the changes not only in the magnitude of the winds, but also in their direction, due to the weakened neutral winds in the G-TING model.

5.2. Disturbed Periods

[26] Compared to quiet periods, much larger changes are observed in the thermosphere during disturbed geomagnetic conditions. The effects on the neutral winds are quite large and, unlike the quiet time effects, they are much more noticeable at high latitudes than at low latitudes (Figure 4a). In the auroral region, plasma convection is significantly enhanced due to the increased magnetospheric electric field during disturbed periods. The resulting, strongly convecting plasma interacts with neutrals, producing much larger Joule heating and stronger neutral winds, compared with the quiet time conditions, which makes the auroral thermosphere much more sensitive to the ionospheric plasma density changes. In the northern hemisphere, the auroral neutral winds from the G-TING model show significantly stronger anti-sunward winds across the polar cap than those from the S-TING model. Quite noticeable differences also occur in the morning sectors. Here the influence of the sunward plasma convection on the neutral motion is noticeable in the G-TING model while it is negligible in the S-TING model. These changes of the neutral winds are mainly caused by the stronger interaction of the ionospheric plasma with neutrals due to the increased plasma densities in the auroral region in the G-TING model. In the southern hemisphere, however, the changes to the neutral winds are minimal. Note that the interpretation of the changes in the neutral winds, particularly in the auroral region, should also consider temperature changes. The temperature shows large changes in the northern hemisphere, producing significant pressure gradient changes, but negligible effects in the southern hemisphere in our simulation study.

[27] The large increases of neutral temperature in the northern hemisphere in the G-TING model can be explained by the enhanced Joule heating rate due to the increased auroral electron densities (Figure 6). In general, the enhanced electron densities increase Joule heating by increasing the Pedersen conductivity while reduced electron densities decrease Joule heating by decreasing the conductivity (see equation (2)). In the northern hemisphere, the enhanced Joule heating in the G-TING model significantly increased the temperature by up to about 200 °K in most parts of the polar region. In the southern hemisphere, however, the Joule heating decreased on the nightside while it mostly increased on the dayside, which results in only small net temperature changes over the auroral region.

[28] In this study the electron density changes have not been applied to *E*-region altitudes, but only to the *F*-region and above. Hence our results of the neutral temperature changes at the z = 2 pressure level in Figure 6 are not directly influenced by heating changes in the *E*-region. Figure 7 shows the altitude profiles of the Joule heating rates per unit volume (in the unit of $erg \cdot sec^{-1} \cdot cm^{-3}$: left panel) and per unit mass or particle (in the unit of $°K \cdot s^{-1}$: right panel) from the S-TING model at the time and location indicated in the figure. The dashed and solid lines represent the heating rates for the quiet (0000UT) and disturbed (2300UT) times, respectively. The altitude profiles of the heating rates show that, although the energy transferred from the magnetosphere is mostly deposited into the *E*-region (left panel), the energy received by individual neutral particles can peak in the *F*-region (right panel), particularly for the quiet time (0000UT), because of decreasing neutral density with altitude [*Thayer and Semeter*, 2004]. This indicates that the energy transfer between the magnetosphere and IT system that occurs in the *F*-region can also be critical in determining the thermal (and therefore dynamical) structure of the upper atmosphere, although the total energy transfer is much smaller than in the *E*-region.

[29] One interesting aspect of this thermal transfer is the diminished role that energetic particle precipitation plays in it. *Rodger et al.* [1992] demonstrated that a clear signature of the ion convection pattern was seen in the high-latitude electron densities at the F_2 peak. This indicated that the majority of the ions that were seen at high latitudes had been advected from elsewhere. A plausible mechanism for this is that the electrons that are swept across the pole from the day side by the ion convection pattern form boundary blobs [*Schunk and Nagy*, 2000]. Thus the potential pattern plays two roles in producing the thermal input at the F_2

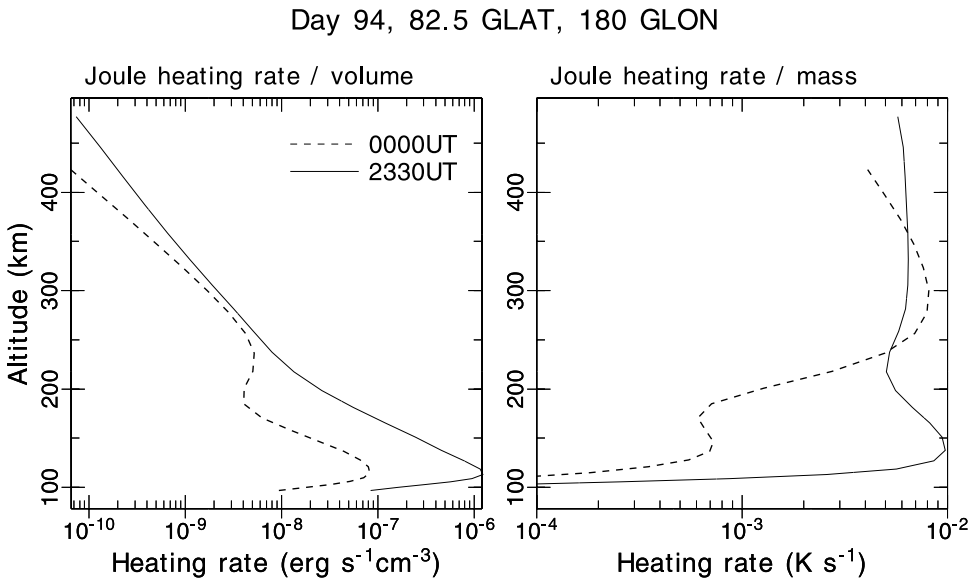

Figure 7. The altitude profiles of the Joule heating rates per unit volume (in the unit of erg·sec^{-1}·cm^{-1}: left panel) and per unit mass or particle (in the unit of °K·sec^{-1}: right panel) at the spatial and temporal conditions indicated in the figure. The dashed and solid lines represent the heating rates for the quiet (0000UT) and disturbed (2300UT) times, respectively.

peak. First, it provides a significant portion of the ions through advection, and second, it provides the momentum for collisions with the neutrals. As a consequence of this behavior, the ion convection pattern is relatively more important compared to the particle precipitation near the F_2 peak than it is at lower altitudes.

[30] During disturbed periods, the neutral composition (O/N_2 ratio) is relatively small in the high-latitude regions compared with the lower-latitude regions (which is called neutral composition bulge; *Prölss*, 1981), since the upwelling of the neutral atmosphere occurs in the high-latitude region as a result of auroral heating. In our results, the composition bulge is relatively stronger in the G-TING model than the S-TING model, particularly in the northern hemisphere, as a consequence of large temperature increases. However, the observed increases of the nighttime O/N_2 ratio in the southern hemisphere cannot be explained by simply considering temperature changes alone and it will require further detailed analysis of the governing physical parameters in the model, which is beyond the scope of the present work.

6. Conclusions

[31] In order to study the effects of the ionospheric plasma density changes on the thermosphere in the coupled thermosphere-ionosphere model, we have replaced the plasma densities in the TING model with the electron densities from the GAIM model above the z = 0 pressure level (~230 km) during 1–4 April 2004 period and observed how the thermosphere reacts to these changed plasma densities.

[32] During quiet times there were noticeable effects on the neutral winds both at low and high latitudes (Figure 3). From this result of our study, it was confirmed that the ionospheric plasma imposes a fairly noticeable drag force on the neutral motion at low latitudes, which was quite clear in the changes of the zonal wind component due to the changed plasma densities (Figure 3a). Auroral plasma density is also a critical factor in determining how neutral motion responds to the ionospheric plasma convection (Figure 3b). However, other thermospheric parameters, such as the neutral temperature and composition, are hardly affected by the changed plasma densities.

[33] During disturbed times the ionosphere-thermosphere interactions in the *F*-region get stronger as the ionospheric plasma convection is enhanced with increasing geomagnetic activity and the interactions become more sensitive to plasma density changes. In addition to the ion drag effects, compared with the quiet conditions, the Joule heating significantly responds to the plasma density changes, which affects not only the neutral winds, but also the neutral temperature and composition (Figures 4, 5, and 6). In particular, considering that the ionospheric plasma density changes were applied only in the *F*-region and above, our results indicate that the magnetospheric energy deposited into the *F*-region can also be important for the upper atmospheric thermal and dynamical structures, despite the fact that the total energy deposited into this region is much smaller than the energy deposited into the *E*-region (Figure 7). We also indicate that the morphology of this energy input can be different from that at lower altitudes because of the importance of plasma transport near the F_2 peak.

[34] Finally, it is well recognized that the thermospheric parameters, such as neutral winds, composition, and temperature, are crucial to the calculation of ionospheric parameters in ionospheric modeling studies. Since the ionospheric parameters are also vital to the determination of thermospheric parameters, as shown partially in our results, the importance of the ionosphere should be re-emphasized in thermospheric modeling studies.

[35] **Acknowledgments.** This material is based upon work supported in part by CISM, which is funded by the STC Program of the National Science Foundation under Agreement Number ATM-0120950. The National Center for Atmospheric Research is sponsored by NSF. The work at Utah State University was supported by NSF grant ATM-0533453. G. Jee also acknowledges support from project PE07030 funded by the Korea Polar Research Institute.

[36] Zuyin Pu thanks Shunrong Zhang and another reviewer for their assistance in evaluating this paper.

References

Buonsanto, M. J. (1999), Ionospheric storms: A review, *Space Sci. Rev.*, *88*, 563–601.

Cierpka, K., M. J. Kosch, M. Rietveld, K. Schlegel, and T. Hagfors (2000), Ion-neutral coupling in the high-latitude F-layer from incoherent scatter and Fabry-Perot interferometer measurements, *Ann. Geophys.*, *18*, 1145–1153.

Deng, W., T. L. Killeen, and A. G. Burns (1991), The flywheel effect: Ionospheric currents after a geomagnetic storm, *Geophys. Res. Lett.*, *18*, 1845–1848.

Deng, W., T. L. Killeen, A. G. Burns, R. G. Roble, J. A. Slavin, and L. E. Wharton (1993), The effects of neutral inertia on ionospheric currents in the high-latitude thermosphere following a geomagnetic storm, *J. Geophys. Res.*, *98*, 7775–7790.

Garriott, O. K., and H. Rishbeth (1963), Effects of temperature changes on the electron density profile in the F2-layer, *Planet. Space Sci.*, *11*, 587–590.

Hardy, D. A., M. S. Gussenhoven, and D. Brautigam (1989), A statistical model of auroral ion precipitation, *J. Geophys. Res.*, *94*, 370–392.

Hedin, A. E., N. W. Spencer, M. A. Biondi, R. G. Burnside, G. Hernandez, and R. M. Johnson (1991), Revised global model of thermospheric winds using satellite and ground-based observations, *J. Geophys. Res.*, *96*, 7657–7688.

Heelis, R. A., J. K. Lowell, and R. W. Spiro (1982), A model of the high-latitude ionospheric convection pattern, *J. Geophys. Res.*, *87*, 6339–6345.

Heppner, J. P., and N. C. Maynard (1987), Empirical high-latitude electric field models, *J. Geophys. Res.*, *92*, 4467–4489.

Kelley, M. C. (1989), *The Earth's Ionosphere*, Academic Press, San Diego.

Killeen, T. L. (1987), Energetics and dynamics of the Earth's thermosphere, *Rev. Geophys.*, *25*, 433–454.

Killeen, T. L., and R. G. Roble (1984), An analysis of the high latitude thermospheric wind pattern calculated by a thermospheric general circulation model: Momentum forcing, *J. Geophys. Res.*, *89*, 7509–7522.

Lyons, L. R., T. L. Killeen, and R. L. Walterscheid (1985), The neutral "flywheel" as a source of quiet-time, polar cap currents, *Geophys. Res. Lett.*, *12*, 101–104.

Maruyama, N., S. Watanabe, and T. J. Fuller-Rowell (2003), Dynamic and energetic coupling in the equatorial ionosphere and thermosphere, *J. Geophys. Res.*, *108*(A11), 1396, doi:10.1029/2002JA009599.

Prölss, G. W. (1981), Latitudinal structure and extension of the polar atmospheric disturbance, *J. Geophys. Res.*, *86*, 2385–2396.

Prölss, G. W. (2004), Physics of the Earth's space environment: An introduction. *Springer-Verlag*, Berlin Heidelberg.

Rishbeth, H. (1979), Ion-drag effects in the thermosphere, *J. Atmos. Sol. Terr. Phys.*, *41*, 885–894.

Rishbeth, H. (1997), The ionospheric E-layer and F-layer dynamos-A tutorial review, *J. Atmos. Sol. Terr. Phys.*, *59*, 1873–1880.

Rishbeth, H. (1998), How the thermospheric circulation affects the ionospheric F2-layer, *J. Atmos. Sol. Terr. Phys.*, *60*, 1385–1402.

Rishbeth, H. (2002), Whatever happened to superrotation?, *J. Atmos. Sol. Terr. Phys.*, *64*, 1351–1360.

Rishbeth, H., and R. Edwards (1989), The isobaric F2-layer, *J. Atmos. Sol. Terr. Phys.*, *51*, 321–338.

Rishbeth, H., C. F. Muller-Wodarg, L. Zou, T. J. Fuller-Rowell, G. H. Millward, R. J. Moffett, D. W. Idenden, and A. D. Aylward (2000), Annual and semiannual variations in the ionospheric F2-layer: ll. Physical discussion, *Ann. Geophys.*, *18*, 945–956.

Roble, R. G., E. C. Ridley, A. D. Richmond, and R. E. Dickinson (1988), A coupled thermosphere/ionosphere general circulation model, *Geophys. Res. Lett.*, *15*, 1325–1328.

Rodger, A. S., R. J. Moffett, and S. Quegan (1992), The role of ion drift in the formation of ion troughs in the mid- and high-latitude ionosphere-A review, *J. Atmos. Sol. Terr. Phys.*, *54*, 1–30.

Scherliess, L., R. W. Schunk, J. J. Sojka, D. C. Thompson, and L. Zhu (2006), The USU GAIM Gauss-Markov Kalman filter model of the ionosphere: Model description and validation, *J. Geophys. Res.*, *111*, A11315, doi:10.1029/2006JA011712.

Schunk, R. W., and A. Nagy (2000), *Ionospheres: Physics, Plasma Physics, and Chemistry*, Cambridge Univ. Press, New York.

Schunk, R. W., et al. (2004), Global Assimilation of Ionospheric Measurements (GAIM), *Radio Sci.*, *39*, RS1S02, doi:10.1029/2002RS002794.

Thayer, J. P. (2000), High-latitude currents and their energy exchange with the ionosphere-thermosphere system, *J. Geophys. Res.*, *105*, 23,015–23,024.

Thayer, J. P., and J. Semeter (2004), The convergence of magnetospheric energy flux in the polar atmosphere, *J. Atmos. Sol. Terr. Phys.*, *66*, 807–824.

Thompson, D. C., L. Scherliess, J. J. Sojka, and R. W. Schunk (2006), The Utah State University Gauss-Markov Kalman filter of the ionosphere: The effect of slant TEC and electron density profile data on model fidelity, *J. Atmos. Sol. Terr. Phys.*, *68*, 947–958.

Titheridge, J. E. (1968), The maintenance of the night ionosphere, *J. Atmos. Sol. Terr. Phys.*, *30*, 1857–1875.

Titheridge, J. E. (1995), Winds in the ionosphere-A review, *J. Atmos. Sol. Terr. Phys.*, *57*, 1681–1714.

Wang, W., T. L. Killeen, A. G. Burns, and R. G. Roble (1999), A high-resolution, three-dimensional, time dependent, nested grid model of the coupled thermosphere-ionosphere, *J. Atmos. Sol. Terr. Phys.*, *61*, 385–397.

Zhang, S. P., and G. G. Shepherd (2000), Neutral winds in the lower thermosphere observed by WINDII during the April 4–5th, 1993 storm, *Geophys. Res. Lett.*, *27*, 1855–1858.

Zhu, X., E. R. Talaat, J. B. H. Baker, and J.-H. Yee (2005), A self-consistent derivation of ion drag and Joule heating for atmospheric dynamics in the thermosphere, *Ann. Geophys.*, *23*, 3313–3322.

A. G. Burns, S. C. Solomon, and W. Wang, High Altitude Observatory, National Center for Atmospheric Research, Boulder, CO, USA.

G. Jee, Korea Polar Reasearch Institute, Icheon, Korea. (ghjee@kopri.re.kr)

L. Scherliess, R. W. Schunk, J. J. Sojka, D. C. Thompson, and L. Zhu, Center for Atmospheric and Space Sciences, Utah State University, Logan, UT, USA.